ARS ADVANCED ROBOTIC SYSTEMS INTERNATIONAL

A Biologically Based Chemo-Sensing UAV for Humanitarian Demining

Sergi Bermúdez i Badia[1,2]; Ulysses Bernardet[2]; Alexis Guanella[1]; Pawel Pyk[1] & Paul F.M.J. Verschure[2,3]

[1] Institute of Neuroinformatics, Uni / ETH Zurich, Winterthurerstrasse 190, CH-8057 Zurich, Switzerland &
[2] SPECS, Technology Department, Universitat Pompeu Fabra, Ocata 1, 08003, Barcelona, Spain &
[3] Institució Catalana de Recerca d'Estudis Avançats (ICREA)
Corresponding author E-mail: sergi.bermudez@upf.edu

Abstract: *Antipersonnel mines, weapons of cheap manufacture but lethal effect, have a high impact on the population even decades after the conflicts have finished. Here we investigate the use of a chemo-sensing Unmanned Aerial Vehicle (cUAV) for demining tasks. We developed a blimp based UAV that is equipped with a broadly tuned metal-thin oxide chemo-sensor. A number of chemical mapping strategies were investigated including two biologically based localization strategies derived from the moth chemical search that can optimize the efficiency of the detection and localization of explosives and therefore be used in the demining process. Additionally, we developed a control layer that allows for both fully autonomous and manual controlled flight, as well as for the scheduling of a fleet of cUAVs. Our results confirm the feasibility of this technology for demining in real-world scenarios and give further support to a biologically based approach where the understanding of biological systems is used to solve difficult engineering problems.*

Keywords: *UAV, demining, autonomous control, localization, biologically based, chemosensing*

1. Introduction

During wars and even many years after their end, one of the longest lasting effects for the civil population is the one caused by antipersonnel mines, cluster bombs and other explosive devices that remain active even decades after the conflict has ended. These weapons, usually simple and cheap to manufacture, are widely used and are very easy to deploy over large areas. As a consequence, there are about 100 million active landmines distributed across areas of previous conflicts that cause unintended injury to more than 26,000 people a year (Gooneratne, 2004). Landmines have a high negative economical, medical and social impact on the local population and their removal is costly, highly time consuming and extremely dangerous. Yet demining is a necessary step for the affected populations to recover.

In order to tackle this problem we believe that three complementary and parallel research areas have to be considered: Firstly, a robotic platform has to be developed that is suitable to work in human non-accessible or unspecified environments and offers the user the safest possible operation. Secondly, among the great number of technologies of potential use to this problem, an appropriate sensor technology has to be employed. And finally, there is a need for an efficient explosive localization strategy that is not only able to locate possible explosive artifacts but that performs this task in a highly efficient way. Often ignored, efficiency can become the most relevant and important issue when the mined areas are not well defined or cover a very large area, or when it is urgently required to transport humanitarian aid through potentially mined areas.

1.1. Conventional methods presently used

Manual demining is still the most broadly used method for landmine detection and neutralization (Habib, 2002; O'Malley, 1993). Its effectivity depends essentially on the sensor technology used, ranging from metal detectors, electromagnetic, acoustic and seismic methods to biological sensors and the properties of the target mine (see Bruschini et al. (1998) and Gooneratne et al. (2004) for review).

Mine clearing machines are usually military devices specially adapted to unearth and detonate explosives. These devices cause enormous environmental damage and do not achieve the same accuracy as manual demining (Habib, 2002). Alternatively, to assist operators, many robotic platforms have been developed, from legged robots to helicopters (Gonzalez de Santos, 2002; Marques, 2002; Nicoud, 1995; Santana, 2005). However, the robot based solutions usually show worse performance than alternative solutions and still require human supervision due to their lack of autonomy. So far, biological sensors, i.e. the use of animals, provide the highest accuracy and safety standards (Bromenshenk, 2003; Fjellanger, 2002; Verhagen, 2006). Dogs and rats have been trained to detect landmines, triggering specific behaviors when a landmine is found. Similarly, bees can also be trained to detect mines. Bees are easier to train and to deploy, and their distribution over a mined field provides a map of the distribution of leaking mines

(Bromenshenk, 2003). However, complex systems have to be developed to measure these distributions.

1.2. A blimp based chemo-sensing UAV.

The use of Unmanned Aerial Vehicle (UAV) technology provides a terrain independent solution and is essentially suited not to trigger mines during the clearing operation. We have developed a blimp based UAV as robotic platform for chemical mapping, search and localization. This platform allows for both high speed displacement and the possibility of slow and low altitude inspection (See Pearce et al. (2004) for a review). This is important because the coverage area is defined mainly by the speed of the robot. A dirigible type platform is a cheaper and intrinsically more stable platform that requires a simpler control layer than planes or helicopter based UAVs. Moreover, model-sized UAVs have short flight times and the time constants describing their dynamics are very short. Therefore, due to the difficult dynamics these devices are inherently unstable and tremendously demanding on the flight control side. However, by now impressive solutions to the autopilot problem exist and are commercially available (Nelson, 1989). In addition, a blimp has a considerable payload compared to helicopter or fixed wing based UAVs, which allows additional on board instrumentation and sensing devices.

Learning from the best sensing machinery - biological systems - we propose to use a metal-thin oxide artificial nose sensor (Alpha MOS SA, France) combined with the current understanding of the odor localization mechanisms of one of the most optimized chemical detection systems known to man, the male moth. The goal is to perform localization using the chemical plumes produced by leaking explosives, the same way dogs, rats and bees do. In addition to an extraordinary sense of smell, this biological system is of particular interest because of its ability to track minute odor cues over a long distance (more than 1km). Based on our study of this preparation, we aim at developing more effective explosive detection and localization (Hansson, 2002). The use of metal-thin oxide technology offers a broad sensitivity to volatile compounds that can be used in real-time chemo-sensing tasks (Lilienthal and Duckett, 2003; Lilienthal and Duckett, 2004; Pyk, 2006).

2. Methods

2.1. cUAV infrastructure

Our custom developed blimp based outdoor cUAV comprises a PVC blimp hull filled with helium (4.5m long, 1.2m diameter, 6m3 volume, with a payload of approximately 3000 g) that is propelled by 4 independent DC motors fixed to a rigid carbon fiber frame (weight approx. 3000g) (Fig. 1). In the evolution of the design we have tried to optimize the stability and maneuverability of the platform as well as its payload and size.

Our cUAV is smaller and more powerful when compared to standard outdoor blimp platforms. The DC motors with neodymium magnets generate approximately 160W each, i.e. an approximate thrust of 620G per propeller. However, this low mass/power ratio results in a more unstable platform than conventional blimps, although faster in dynamic responses.

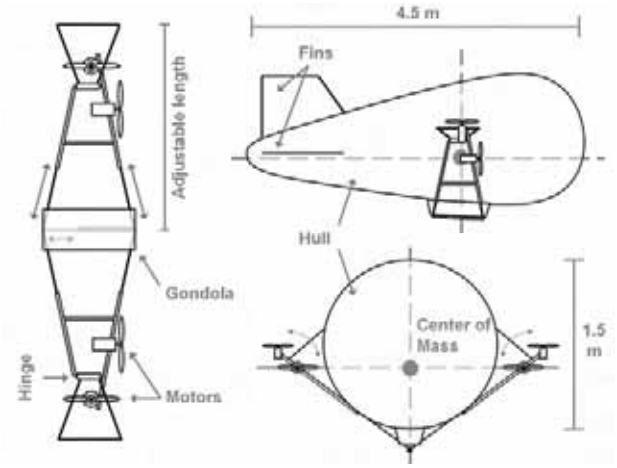

Fig. 1. Design of the blimp based cUAV. The motor frame consists of 2 pairs of motors (for independent control of altitude and translation) mounted on a carbon fiber frame that builds around the hull of the blimp. A hinge mechanism and the adjustable length of the motor frame make it easy to adjust to different blimp sizes.

Conventional motor controllers for dirigibles are based on 2 unidirectional motors attached to the blimp through a gondola in the lower part of the hull. The motors are mounted on a common short axis which is steered via a servo motor to change the angle relative to ground, allowing both altitude and translation/rotation control requiring minimal infrastructure. To minimize instabilities, because of the weak attachment of the gondola and hull, the separation of the 2 motors is small and therefore a big force is needed to produce relatively small torque forces to rotate the cUAV. Consequently, this motor configuration prevents the UAV from performing some determined maneuvers and applies forces at a point far from the Center of Mass (CM) provoking undesired torque. Given the short time constants of our cUAV, due to the mass/power ratio, these conventional solutions cause an oscillatory roll, pitch and yaw behavior. In our novel design, we maximized stability and maneuverability by applying the generated motor forces as close as possible to the CM (Fig. 1).

The distance between the pair of motors responsible for rotatory maneuvers is significantly increased since the motor structure is constructed around the hull as opposed to be attached exclusively to its lower part. This means that greater torque forces can be generated by the

same motors, resulting in faster rotatory responses. The motors are mounted on a carbon fiber structure that can fit different hull sizes and be finely adjusted thanks to its extension mechanisms. Additionally, a set of fins (of approx. 0.2 m^2) are used as a passive stabilization mechanism. Thus, the redesign of the motor structure allows our smaller and more powerful cUAV to be an intrinsically more stable platform, with a better maneuverability and a faster response than standard off the shelf solutions.

2.2. Sensors and electronics

One of the advantages of a blimp based cUAV compared to helicopter and fix wing cUAVs is the payload. Our cUAV can carry a number of sensors for conventional control, monitoring and analysis such as a GPS, a 3D compass, a 3D accelerometer, a gyroscope, altimeters, etc. The control board is realized using a network of four AVRMega32 controllers (ATmega32L, Atmel, San Jose, CA, USA, www.atmel.com) that are interfacing a number of sensors (GPS, 3D compass, altimeters, etc), the motor control board, and the communication system (a 2.4GHz transceiver AC1524 from Aerocomm, Lenexa, USA). All these sensors are connected to a common bus (TWI – Two-Wires Interface) and allow for easy system interfacing and expansion of additional modules such as chemo-sensors. The total weight of the electronics, including transceiver and all sensors, is 90g, and a size of 80x100mm (Fig. 2).

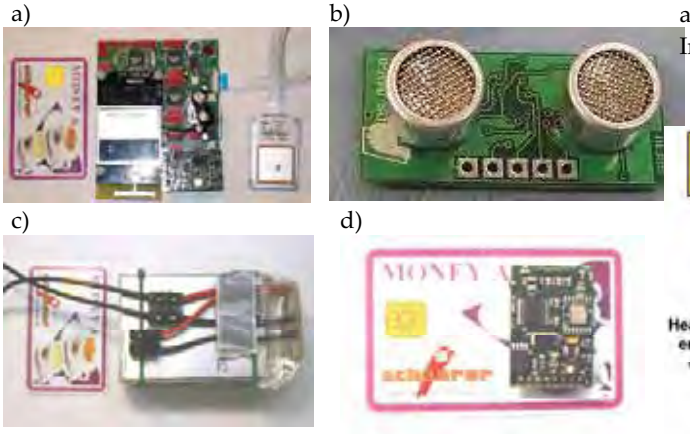

Fig. 2. Electronic components and sensors of the cUAV. a) The control board uses AVRMega32 Atmel controllers and interfaces GPS, 3D compass, altimeters (barometric and ultrasonic), motor control and communication. Dimensions: 80x100mm. b) The sonar altitude sensor uses 5V, requiring 15mA. The sampling frequency is 40KHz with a range of 3cm to 6m. Dimension: 32mm x 15mm x 10mm. c) cUAV lithium-polymer rechargeable batteries. d) Digital 3d magnetic compass, measures heading, yaw and pitch angle with a resolution of 0.1 deg, heading accuracy 1 deg, sampling rate 8 Hz.

The cUAV uses Lithium-Polymer rechargeable batteries (KOK 3270, Kokam, Kyunggi-do, Korea, www.kokam.com) that provide up to 5 times higher energy per unit of mass than classic Nickel Cadmium rechargeable batteries (8 cells with a capacity of 13 Ah, provide 7.4V). As a result, autonomy of up to 2 hours can be achieved in moderate wind speeds.

2.3. Autonomous control layer

One major step forward in the development and deployment of the cUAV was the construction of a ground station autopilot. Thanks to the 2.4GHz long range radio link system with our ground station (up to 1 km range), the UAV can be both manually and autonomously controlled by means of a software autopilot. The autopilot software that runs on the ground station generates the appropriate motor commands to move the cUAV to specific GPS coordinates, to produce pre-programmed trajectories or can act as an intermediate control layer connected to the neural simulator **iqr** making sure that the commands are executed with high reliability (Bernardet, 2002).

As for the control of our outdoor cUAV we have investigated a number of control systems: Fuzzy logic, Proportional-Derivative (PD) and Proportional-Integral-Derivative (PID). For testing the different control systems we used a variety of platforms such as a ground based tracked vehicle, an indoor blimp and wheeled version of the outdoor cUAV platform. Preliminary tests on the outdoor cUAV showed that in order to deal with noise or the unavailability of on board detection of wind direction and force, it was necessary to implement a Proportional-Integral-Derivative (PID) control layer (Fig. 3).

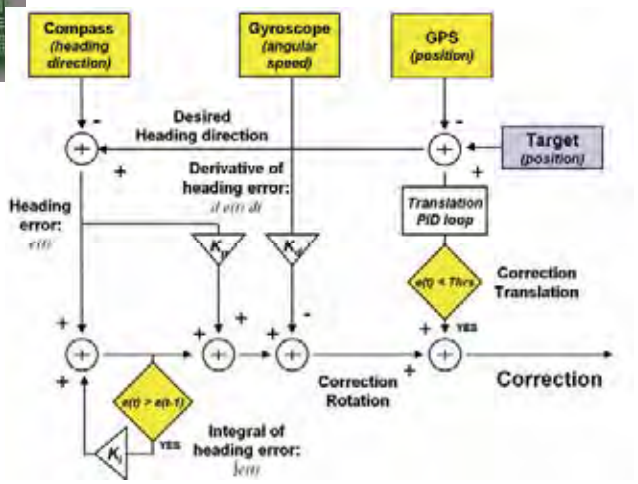

Fig. 3. Schema of the rotation and translation PID control loops implemented on the outdoor cUAV. The described system controls the heading direction. See text for further explanation.

The PID controller is a standard system in control theory and makes use of a feedback loop that aims at bringing a set of measured values of a process to a desired setpoint.

The computational and algorithmic requirements of this controller are simpler and can be more easily tuned to a variety of applications than other algorithms based on optimal control theory (O'Dwyer, 2003). The PID controller compares a measurement with a reference value and computes the difference, i.e. the error. In the processing loop, a correction signal is calculated based on 3 principles: *proportionality* to the computed error, the *integration* of the uncorrected error and a prediction of the future error (*derivative*):

$$Correction = K_p e(t) + K_i \int_{reset} e(t) + K_d \frac{d}{dt} e(t) \quad (1)$$

where $e(t)$ represents the error measured and K_p , K_i and K_d are constants used to tune the PID control loop.

In the particular case of our outdoor cUAV, and due to the physical independence between the altitude and translation/rotation control, altitude has been treated separately with an independent PD controller. The PD controller for altitude was based on the readings of an ultrasound based altimeter (See 2.2). The altitude motor correction commands are proportional to the difference between sensor readings and the desired set point and its derivative:

$$Correction_{altitude} = K_p e(t) + K_d \frac{d}{dt} e(t) \quad (2)$$

where $e(t)$ is the altitude error and K_p and K_d *are* the proportionality gains, i.e. 3 and 2 in our control loop.

The full PID controller was applied only to the translational and rotational control, where the variable effect of the wind made it necessary to prevent over- and undershoot. Although both rotation and translation are driven by the same motor system (the 2 horizontally oriented motors) they are computed in independent control loops (Fig. 3). In order to minimize the interference between the two above mentioned control loops, the translation control was only activated when the angular error in the heading direction was below a specific angular threshold (*Thr*):

$$Correction_{Horizontal} = \begin{cases} Correction_{Rotation} + Correction_{Translation} & if\ e_{heading}(t) < Thr \\ Correction_{Rotation} & if\ e_{heading}(t) > Thr \end{cases} \quad (3)$$

Here $e_{heading}(t)$ represents the error between the desired and the actual heading direction (compass reading), and $Correction_{Rotation}$ and $Correction_{Translation}$ are the independent PID control loops for rotation and translation respectively. The reason to use this approach is that both control loops actuate the same motors, and the actual cUAV heading direction has to be taken into account when translating. Splitting the problem into a first turning and then translating problem minimizes the interference between control loops and simplifies a two degrees of freedom problem, i.e. distance and heading direction, into two one degree of freedom problems.

The PID control loop implemented to adjust the heading direction to the desired setpoint makes use of the on board compass, GPS and gyroscope (Fig. 2, Fig. 3). The GPS data is used to compute the desired heading direction to go to the desired target location from the current one, the compass measurement is used as the controllable variable of the process, and the gyroscope package provides an accurate first and second derivative of the measurement from the compass.

$$\begin{aligned} Correction_{Rotation} &= K_p(SetPoint - Compass(t)) \\ &+ K_i \int_{reset} f(SetPoint - Compass(t)) + K_d \frac{d}{dt}(SetPoint - Compass(t)) \\ &= K_p(SetPoint - Compass(t)) + K_i \int_{reset} f(SetPoint - Compass(t)) - K_d Gyro(t) \end{aligned} \quad (4)$$

with K_p = 0.4, K_i = 0.2 and K_d = 0.2, and being *Gyro(t)* and *Compass(t)* the gyroscope and compass measurements respectively. To avoid the accumulation of error over time due to the integration term, the integration is reset (t_{reset}) when the compass measurement and desired heading direction are within a confidence interval. In practice, it was convenient to use $f(x)$ in eq. 4 to reduce the overshooting caused by a constant wind force:

$$f(x) = \begin{cases} e_{heading}(t) & if\ e_{heading}(t) \geq e_{heading}(t-1) \\ 0 & if\ e_{heading}(t) < e_{heading}(t-1) \end{cases} \quad (5)$$

Fig. 4. Our cUAV during an autonomous flight using the autonomous control layer.

The translation control loop works analogously to the rotation one described above, with the difference that it uses the distance to the target as the controllable variable of the process. In this case, all measurements rely solely on the GPS reading, from which distance to the target and cUAV speed are computed. To summarize: the autonomous control layer consists of two PID control loops that control rotation and translation and an

additional PD loop for altitude control that are required for the cUAV to perform autonomous flight (Fig. 4)

2.4." Walking moth" robot

To test and evaluate the performance of different odor localization strategies we developed a Plexiglas circular robot with a diameter of 20 cm (Fig. 5a). For locomotion it uses two active wheels (diameter 49 mm) placed on the axis of the robot, each driven by geared motors with a continuous rotation servo (Parallax-Futaba Continuous Rotation Servo, Parallax, Rocklin, CA, USA, www.parallax.com), allowing for in place rotation. To provide balance and stability, a ball caster encapsulated in a holder was used as a third support point. The chemo-sensory boards were placed in the midline of the platform. The movement commands and integrated sensory data are exchanged between the mobile platform and the base station using a Bluetooth module (Bluetooth™ RS232 Class I Industrial Adapter, LinTech, Berlin, Germany, www.lintech.de).

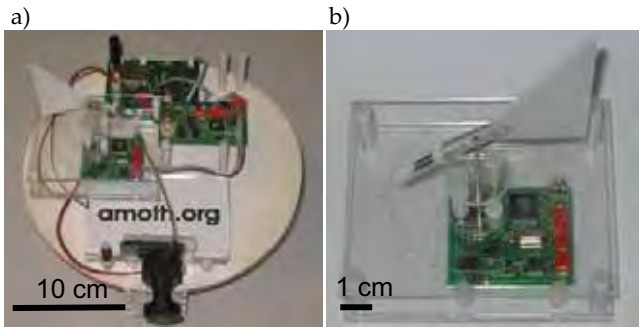

Fig. 5. The walking moth mobile robot platform. a) Our chemo-sensory ground vehicle consisting of, from top to bottom, a control board with a Bluetooth communication module, a chemo-sensor board and the wind direction sensor (diameter 20 cm, height 16 cm). b) The wind direction sensor comprises of a vane that is attached to a rotating shaft fitted with a small magnet. See text for further explanations. Adapted from Pyk et al. (Pyk, 2006).

The robot electronics consist of three custom built boards: a main board, a chemo-sensing board (see 2.5), and a wind direction sensor board. Each of these sensors is served by its own microcontroller. The wind direction was measured with a custom built sensor consisting of a light weight styrophore wind vane that was fitted to a magnetic encoder. The angular position of the shaft was measured using a 2-axial magnetometer (MicroMag2, PNI Corporation, Santa Rosa, USA, www.pnicorp.com). The board is fitted with an ATmega32L microcontroller that calculates the wind direction and interfaces the magnetometer to the robot infrastructure via the TWI bus (Fig. 5b). A microcontroller is responsible for the Bluetooth communication and motor control. All the microcontrollers are connected to a common bus (TWI – Two-Wire Interface). As the cUAV, this robot uses Lithium-Polymer rechargeable batteries (KOK 3270, Kokam, Kyunggi-do, Korea, www.kokam.com) that provide up to 8 hours of continuous operation. Since the batteries are sensitive to discharge and overcharge, the battery status is continuously monitored.

2.5. Chemo-sensor technology

The 6 grid array thin film metal oxide chemo-sensor used (Alpha MOS SA, France) provides a broad spectrum of sensitivity, responding to a wide range of volatile organic compounds (Pyk, 2006) (Fig. 6). The selectivity of individual sensors to different compounds can be controlled by its geometric organization as well as variations in the semiconductor materials and dopants used for manufacture. In this study we used a 6 sensor array where sensors 1-5 were n-type metal oxide semiconductor Tin Oxide (SnO_2), sensors 2 and 4 were doped with catalytic metal additives Palladium (Pd) and Platinum (Pt) respectively. The sensor 6 was a p-type metal oxide semiconductor Niobium Oxide (Nb_2O_5). This technology has relatively low power consumption (approx. 270mW) it provides a high degree of miniaturization. The dimensions of the whole 6 grid array sensory chip are 2 x 3 x 0.38mm (with x length x thickness).

The sensitivity of these sensors can go up to few particles per million (ppm) and has a broad tuning that allows for identification of volatile organic compounds in the air (Eickhoff, 2003; Neubecker, 1997). However, the requirements to detect some explosives such as TNT or DNT goes down to few parts per billion (ppb) (Rose et al., 2005). The bulk resistance of these chemo-sensitive resistors depends upon various physical parameters, such as the surface interaction between odor molecules and the semiconductor material (Nanto, 2003). Thus, volatile chemicals produce different responses on each of the sensors of the grid depending on the particular doping of the sensor. Previous experimental work suggested that the amplitude and the temporal dynamics of the responses of each sensor produce a unique chemical finger print (Pyk, 2006).

The chemo-sensor array package was integrated on a printed circuit board (Fig. 6) that controlled its heating to determine the operating temperature, and sampled the sensor resistance at a frequency of 16.3 Hz. The sensor resistance is converted into voltage and subsequently digitized. In this technology it is interesting to use the fractional change in conductance (FCG) as measure since it is proportional to the chemical concentration. The FCG is computed as follows:

$$FCG(t) = \frac{G_{stimulus}(t) - G_{nostimulus}}{G_{nostimulus}} \quad (6)$$

where $G_{stimulus}(t)$ is the conductance ($1/R$) during the experiment i.e. in the presence of chemical stimuli and

$G_{nostimulus}$ is the mean conductance baseline obtained in the absence of any stimuli. Additionally, this procedure allows us to calibrate the sensor as well as to correct for the sensor response drift over time.

a)

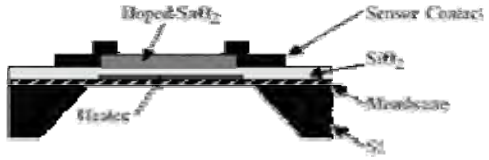

b)

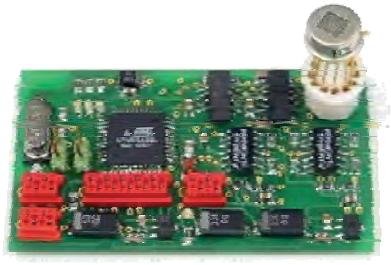

Fig. 6. The 6 grid array thin-metal oxide sensor package. a) Cross-section of the sensor package indicating its parts. The dimensions of a single sensor are 0.18 x 0mm (with x length), with an active area of 0.032 mm². The thickness of the sensitive material is 0.8μm. b) Custom built chemo-sensory board to interface a 6 grid array sensor. The sensor sampling rate is 16.3Hz for each of the 6 sensory channels. Weight: 13.8g, dimensions: 34.5 x 60mm. See text for further explanation. Adapted from Pyk et al.(Pyk, 2006).

2.6. Wind tunnel

All of the mobile robot experiments were performed in a low-cost wind tunnel measuring 3 x 4 x 0.54m that was constructed from wood and transparent plastic sheets (Fig. 7). Four ventilators with independently adjustable speeds at the end of the wind tunnel create negative pressure and suck the air out into an exhaust tunnel. An overhead camera provides the video input to track the robot position over time. For tracking, a custom made general purpose tracking system called AnTS was used.

A solution of fixed concentration of 20% ethanol and distilled water was delivered using an ultrasonic release system (Mist of Dreams, XrLight, Zhongshong City, China) that generates a rapidly evaporating mist at a rate of about 3.33ml min^{-1}, yielding about 0.8ml min^{-1} of ethanol. This vaporizer was boxed in a closed chamber (40 x 40cm) which only exit was through a remotely controlled impeller (CGW/EDF-50, GrandWing Servo-tech C0, Ltd, Taiwan). An average air speed of 0.67m/s was measured with an anemometer placed at the outlet of the wind tunnel and the wind speed and air volume at the inlet was reconstructed from these measurements.

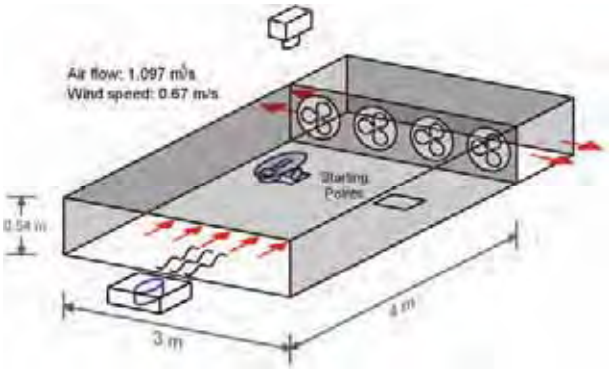

Fig. 7. Schema of the wind tunnel. The wind tunnel is 4 m long, 3m wide and 0.54 m high. 4 ventilators with independently adjustable speeds at the end of the wind tunnel create negative pressure and suck the air out of the wind tunnel into an exhaust tunnel. The odor source (blue), boxed to control the delivery via an impeller, was placed in the middle of the entrance of the wind tunnel in all experiments. The two squares in the wind tunnel mark the two starting points used for the robot experiments. An overhead camera is used to track the robot position over time. Adapted from Pyk et al.(Pyk, 2006).

2.7. Search strategies

Chemical cues, as opposed to be presented in a smooth gradient like signal, usually appear as turbulent plumes. For instance, the highest odor concentration and the instantaneous wind direction in turbulent plumes are cues that not necessarily lead to the odor source, and therefore complex search strategies have to be investigated (Murlis, 1981; Murlis et al., 1992).

It is important to point out that the subsequently described odor localization models are implemented on the neural simulator **iqr** and all the behaviors displayed by the robot are the result of excitatory and inhibitory interactions between neurons that simulate from the moth olfactory periphery neurons (i.e. Antennal Lobe) to the motor responses (i.e. Motor Ganglion). This solution keeps the on board computation to a minimum while not compromising the computational requirements of the neuronal systems that we study.

A number of localization techniques are implemented as neural networks on the mobile platform and the cUAV. These include two basic approaches towards mapping the chemical concentration of an area (random search vs. scanning) and two biologically based localization models (a behavioral and a neural model of the moth chemical search behavior). Additionally, fleet scheduling strategies have been implemented and tested for a fleet of cUAVs.

2.7.1. Simulations: mapping and scheduling

We simulated a fleet of four blimps in a square open field environment of 20x20m². The blimps are modeled as a rigid ellipsoid of revolution with length 1m, height 0.5m and width 0.5m. The model dynamics are derived from the Kirchhoff equations of a rigid body immersed in an

incompressible, irrotational, inviscid fluid (Milne-Thomson, 1973), with 6 degrees of freedom (surge, sway, heave, roll, pitch and yaw) (Zufferey, 2006). Each blimp is equipped with three propellers, one on the front for forward motion, one on the middle, for up and down motion and one on the back, for yaw rotations. The maximum propeller force is 0.04 [N]. The blimps are provided with three sensors, i.e. a GPS, a chemo-sensor and a compass, modeled as perfect sensors.

2.7.2. Robot experiments: behavioral model

This model is solely based on observations of the behavior displayed by the moth during chemotaxis. This model exploits the two behavioral modes observed in previous studies (Baker and Kuenen, 1982; Cardé and Hagaman, 1979; Kennedy et al., 1978; Vickers and Baker, 1994). Male moths tend to show a regular zigzagging behavior called casting when trying to intercept a filament of a pheromone plume. Once the plume is intercepted, moths make an upwind displacement in response to the pheromone contact, known as a surge. Then, if the pheromone filament is lost, moths return to the casting mode.

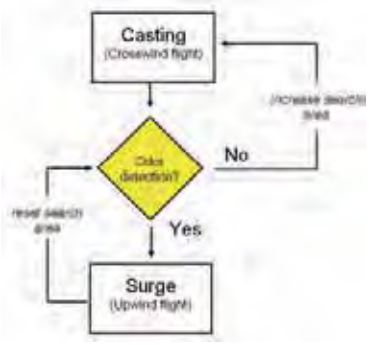

Fig. 8. Block diagram of the studied behavioral model. Two basic behavioral modes are alternated by odor contact; surge defines an upwind displacement whereas casting a zigzag crosswind oriented displacement. The amplitude of the casting behavioral mode is increased over time and only reset by odor contact.

Our particular implementation of this strategy is based on a simulation study which demonstrated that under determined conditions this strategy is close to optimal (Balkovsky and Shraiman, 2002).In that study, the casting behavior is characterized by an increase of the crosswind flight displacement over time, and a short upwind displacement at the extreme position of it. A contact with a pheromone molecule resets the length of the casting displacement and triggers a change to surge mode (Fig. 8). During the robot experiments, the wind direction was estimated using the custom built anemometer (see 2.4), and used by the model to produce the right upwind displacement. Only one chemical sensor was used in the evaluation of this model.

2.7.3. Robot experiments: neural model

As opposed to the previously described model, the neuronal model aims at exploiting the known neural substrate of the moth rather than the observed behavior involved on the chemical search task.

The, so called, Descending Neurons (DN), found in the protocerebum of the moth brain, have dendritic arborizations in the Lateral Accessory Lobe (LAL) of the moth brain and show a high/low firing rate that switches depending on the difference of pheromone concentration in the insect antennae (Kanzaki et al., 1989). Moreover, these DN neurons, called flip/flop neurons, are synchronized with the change of orientation during the zigzag behavior in the odor localization task (Mishima, 1998; Olberg, 1993; Wada and Kanzaki, 2005). Our model includes the principle of these flip/flop neurons to control change in heading direction of the robot according to the difference of the sensed chemical concentration of two on board chemical sensors (Fig. 9a).

a) b)

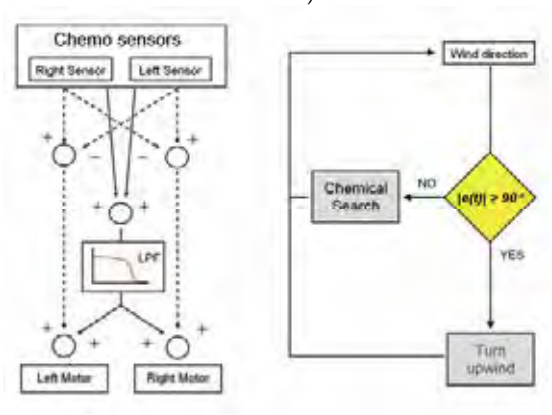

Fig. 9. Diagrams of the proposed neural model. a) Schema of the computations taking place during the chemical search, in which the left/right chemo-sensor responses are compared to produce motor actions. b) Block diagram of the neural model describing the two basic behaviors; a chemical search mode (a) whenever the robot heads at an angle smaller than 90° to the wind direction, and an upwind reorientation whenever else.

The Macro Glomerular Complex (MGC) of the Antennal Lobe (AL) of the moth is a glomerulus solely dedicated to the encoding of pheromone signals (Christensen et al., 1995; Christensen and Hildebrand, 1987; Christensen et al., 1993; Hansson et al., 1991; Kanzaki et al., 1989). The majority of the neurons in the MGC neurons (approximately 85% of the total) are only able to resolve odor pulses of moderate frequencies (up to few Hz) (Christensen and Hildebrand, 1987; Christensen et al., 1993; Lei and Hansson, 1999). It has been suggested that their specific frequency sensitivity matches the characteristics of the plume that carries the odor packages, and therefore the frequency range that carries the odor relevant information and that triggers the

upwind displacement (Murlis, 1981; Murlis et al., 1992). This aspect of the biology is modeled as a Low Pass Filter (LPF) of the readings of the chemical sensors (Fig. 9a).
The wind direction information in this neurally constrained model is solely used to prevent the robot moth from going downwind when the sensed chemical concentration is ambiguous or this information leads to an undesired downwind displacement (Fig. 9b).

3. Results

3.1. Simulations: mapping experiments

Simulation experiments of a fleet of cUAVs were used to investigate two possible mapping strategies with a fleet of cUAVs in a square open field environment of 20x20 m^2. A scan and a random search behavior were analyzed, quantifying the area coverage, time required and the quality of estimation of the distribution of explosive within an area. We computed the trajectories of a fleet of 4 blimps on trials of 50,000 time steps of 0.02 sec., corresponding to flights of 17 minutes (Fig. 10).

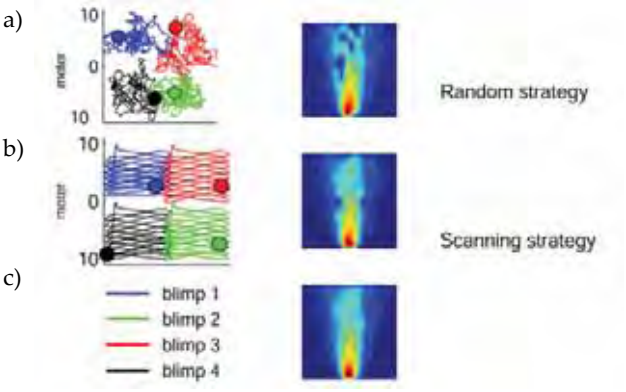

Fig. 10. Left column: trajectories of the blimp fleet for the two different exploration strategies. Circles indicate random initial positions. a) Random search and b) Scanning behavior. Right column: reconstruction of the odor map after an exploration of 17 minutes, for the two different exploration strategies. c) Legend and original odor plume map.

To study which of the exploration strategies is more optimal in terms of area coverage, after 50,000 time steps we computed the percentage of space covered. We discretized the environment into bins of 1 square meter, corresponding approximately to the size of the robots, to compute the area covered by the four robots. For the random strategy, the percentage of space covered was of 81.4 % +/- 5.8 % (mean +/- std). For the scanning behavior, we found a percentage of space covered of 93.3 % +/- 1.2 % (mean +/- std).
To determine the accuracy of an odor map reconstruction, we generated a snapshot of a model odor field, with odor dispersal based on a random walk model, where the stationary distribution can be modeled by a Gaussian distribution (Balkovsky and Shraiman, 2002). The simulated fleet of cUAVs reconstructed this map and its similarity with the original map was computed by means of a correlation measure: random vs. real = 0.968 and scanning vs. real = 0.992.
Although apparently scanning outperforms the random search, when we examine the evolution over time of the previous two measures, the random search shows larger area coverage at the beginning followed by a later saturation whereas the scanning a uniformly increasing area coverage over time (data not shown). Then, the selection of the most convenient search strategy depends on the time available and area size.

3.2. Robot experiments: outdoor mapping

A number of experiments were performed on the university football field (40x80 m.), with an average wind speed of 3 km/h. An ethanol solution was used as odor stimulus. An alcohol water solution was released using an ultrasonic release system that delivers 200 ml h^{-1} of 40% ethanol in water.

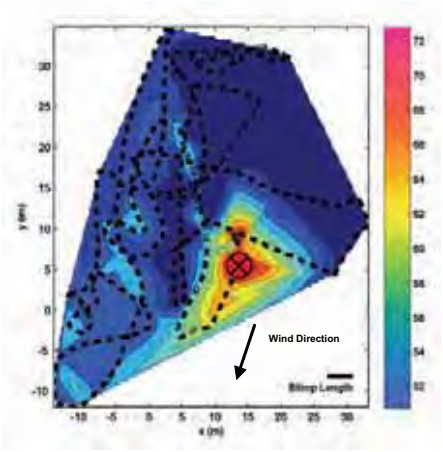

Fig. 11. Demonstration of random search strategy used to create maps of the cUAV chemo-sensor response. The red circle indicates the ethanol odor source position. The colors indicate the response strength of the chemo-sensor. The maximum response of the map distribution reliably indicates the position of the ethanol dispenser. The chemo-sensor response was interpolated using a triangle-based cubic interpolation. The trace length is approx. 310 m.

We implemented and tested the strategies for chemical mapping which were previously evaluated in simulations, i.e. scanning and random search. The goal was to demonstrate the feasibility of reproducing them autonomously with the outdoor cUAV under realistic outdoor conditions (Fig. 11, Fig. 12). Hence, we use the outdoor cUAV experiments to validate the results obtained with the physics based simulation of a fleet of cUAVs.

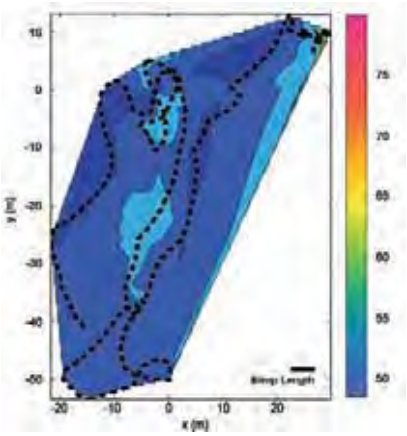

Fig. 12. Demonstration of scanning search strategy used to create maps of the chemo-sensor response. The colors indicate the response strength of the chemo-sensor. In this experiment the odor source was absent. The chemo-sensor response was interpolated using a triangle-based cubic interpolation. The trace length is approx. 160 m.

A set of random search experiments were performed with an active odorant source that allowed us to get a distribution map of the ethanol concentration and evaluate its performance. Indeed we observe that the random search condition correctly defines the location of the ethanol source with a relatively short flight trajectory (Fig. 11).

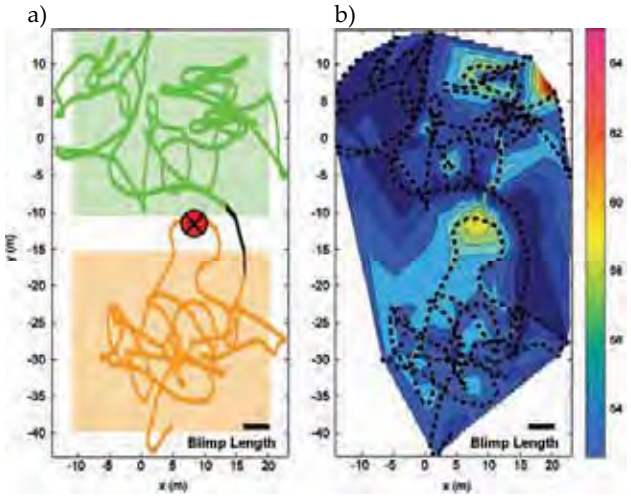

Fig. 13. Example of the cUAV Fleet scheduling task using random sampling of the area. a) A single cUAV performs a sequential mapping of 2 non-overlapping areas 30 x 25 m. (green and orange shaded areas). The red circle indicates the ethanol odor source location, orange and green traces the robot random search behavior, and the black trace the transition from green to orange areas. b) Resulting chemical map after the scheduling task. The colors are indicating response strength of the chemo-sensor. The chemo-sensor response was interpolated using a triangle-based cubic interpolation. The trace length is approx. 290 m.

The scanning strategy was also implemented and demonstrated autonomously on the cUAV (Fig. 12). These two results demonstrate on the one hand the reliability of the hardware infrastructure of the cUAV, and on the other hand that it can produce fully autonomous chemical localizations based on two predefined sets of behaviors, random search and scanning.

However, when source localization is required over very large areas, it is unfeasible to assume that a single cUAV can perform this task alone. For this reason we investigated the possibility of scheduling of a fleet based on a division of the area to explore among the cUAVs. Thus, we made a set of experiments where the cUAV was assigned to examine a certain area using the random search strategy (Fig. 13a, green area) and subsequently rescheduled to move to another non-overlapping area (Fig. 13a, orange area). Indeed, the cUAV is able to sequentially examine non-overlapping areas autonomously and create a consistent chemical map of the sensed ethanol distribution (Fig. 13b).

3.3. Robot experiments: indoor odor localization

Usually, the role of odor localization is reduced to perform a full coverage of an area although it becomes crucial when mined areas are not defined or are very large and it is not possible to explore the complete area. In this case, rather than mapping a large potentially mined area, it is more important to be able to locate individual or clusters of mines. Note that mapping is not equivalent to localization, even though mine localization from a mapped area is a much easier task than localization alone. Inspired by the extraordinary performance of biological systems in this task, we investigated in a custom built wind tunnel (see 2.6) the performance of two biologically based models of the moth chemical search behavior (see 2.7). which were based on different biological criteria, where the first was exclusively based on behavioral observations using only one chemical sensor, and the second was based on the known neural substrate making use of two chemical sensors (Fig. 14).

Using a custom mobile robot ("walking moth") running at a speed of about 10 cm/s (see 2.4) interfaced with the neural simulator **iqr** we tested two biologically based models (see 2.7) in our wind tunnel infrastructure (see 2.6). The two implemented and tested models were able to reliably find an odor source under very controlled conditions in which a field chemical plume was simulated consistent with our previous studies (Pyk, 2006). In the behavioral model, the two modes, surge and casting, can be clearly distinguished (see 2.7), and their combination with an odor contact driven switch between those two modes successfully leads the robot to the source of odor. However, in the neural model, the robot displays straighter traces than the previous model although still with zigzag segments.

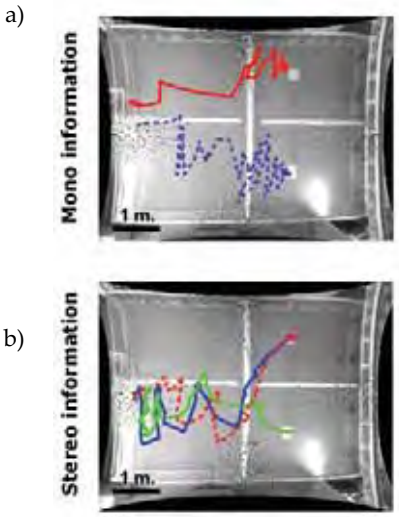

Fig. 14. Chemical search traces of the two studied biologically based models in our custom made wind tunnel. a) Representative examples of traces generated by the behavioral model exclusively using one chemical sensor. b) Representative examples of traces generated by the neural model that makes use of stereo chemical information. See text for further information.

To evaluate the performance, 40 robot runs of the behavioral model and 60 of the neural model were performed. For that, we used the simplest possible criteria, i.e. the shorter the search time and the smaller the localization error, the better the performance.

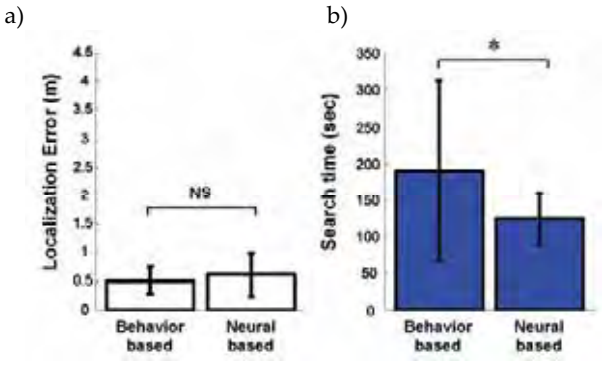

Fig. 15. Performance comparison of the two biologically based models. Comparison of the localization error (a) and (b) average search time on both systems. A total of 100 robot experiments were performed for both conditions. See text for further explanation.

Surprisingly, even though the two models rely on very different information and processing systems to locate odors, both show an equivalent mean localization error. In this scenario, where the largest distance to the source in the wind tunnel is 4.3 m, the obtained error for both models was about 0.5 m., being not significantly different (2 sample t-test, $p > 0.05$) (Fig. 15a). However, the performance difference is clearer when comparing the mean search times for the two models. In this case, the neural based model outperforms with more than one minute, 31% of the total task duration, the performance of the behavior based model (2 sample t-test, $p < 0.05$) (Fig. 15a). The best performing biologically based model showed a mean search time of about 2 minutes whereas the total time of a full scan of the wind tunnel at the used robot speed would take about 5 minutes. Moreover, this time difference increases exponentially with the size of the search area.

4. Conclusions

We have presented a biologically based solution to the detection problem in demining exploiting the benefits of using a chemo-sensing UAV platform, an artificial nose sensor and a neuroethological analysis on biological systems that perform this task.

Our novel robotic blimp based UAV platform equipped with standard sensory systems and an artificial nose (a thin-metal oxide chemical sensor) has a special set of properties such as terrain independence, fast maneuverability and capable of slow and low altitude inspection, does not trigger mines, payload for additional sensory equipment, that make it very well suited to the humanitarian demining task. In addition, its particular motor configuration makes it more stable than conventional blimp based UAVs and we developed a control layer that provides with fully autonomous and manual control. This approach minimizes the risk and human supervision while still offering fully manual control if required. In addition, the control layer serves as an intermediate layer between our large-scale neural simulations and the cUAV, assuring that the commands from the neural models are reliably executed by the cUAV. Among the limited number of sensor technologies applied to demining that can be carried on a UAV, we used a metal thin oxide sensor since it offers a broad sensitivity to volatile compounds that can be used for detection and classification of chemicals in real time although the scope of this research does not limit to this sensor technology.

In this study, we compared different exploration strategies implemented on a simulated fleet of four blimps and on a real cUAV. A random search strategy seems to be the simplest strategy to map an environment in the shortest period of time, whereas the scanning behavior leads to slightly better results but requires a longer period of time. These strategies were implemented to be autonomously generated by our cUAV infrastructure to map the chemical concentration of large areas. Moreover, we demonstrated scheduling of a number of cUAVs over large areas to map non-overlapping areas. The obtained maps are a reliable estimation of the chemical distribution of the explored areas and can be used to perform localization of multiple chemical sources such as land mines, cluster bombs or explosives in general.

As opposed to systematically examine an area, and inspired by biology, we propose a way to intelligently search where the mines are. We studied two localization strategies in a wind tunnel to simulate realistic chemical plumes as they are produced by leaking explosives. We have shown that both biologically based localization strategies reduce significantly the search time compared to scanning and that the neural based model was significantly faster. This result suggests that in order to mimic or fully understand strategies such as the moth chemotaxis, it is not sufficient to solely reproduce the behavior but it is even more important to understand the neural mechanisms that generate those behaviors.

5. Outlook

The presented cUAV is an ideal and low-cost outdoor platform to test in the field the studied chemical search models in the wind tunnel, and will be further investigated.

This study used ethanol as the stimulus for the experiments; however, explosives are made of more complex substances. Thus, an analysis of the sensitivity of our artificial nose to real explosive compounds plus the implementation of a robust odor classifier is a necessary step towards mine clearance. Moreover, odor cues are carried in turbulent air structures that change over time depending on many aspects such as environmental configuration, vegetation, wind speed, etc. The effect of those factors on the localization strategies has to be studied and characterized to define the working conditions. Nonetheless, the overall behavioral competence of our system is independent of the details of the sensing technology.

The cUAV can be augmented by including an on-board visual reactive layer (collision avoidance, course stabilization) based on our work on insect based models that would reduce the computational requirements of the autonomous control layer yet providing further functionality (Bermúdez i Badia, 2005; Bermúdez i Badia, 2004).

6. Acknowledgements

We thank P. Knuesel for his contribution to the software infrastructure. This research is supported by the EU and BBW (Grant "A Fleet of Artificial Chemo sensing Moths for Distributed Environmental Monitoring (AMOTH)" to PFMJV, funded under the IST Future and Emerging Technologies Programme (IST-2001-33066)

7. References

Baker, T. C., and Kuenen, L. P. S. (1982). Pheromone source location by flying moths: a supplementary non-anemotactic mechanism. Science *216*, 424-427.

Balkovsky, E., and Shraiman, B. I. (2002). Olfactory search at high Reynolds number. Proc Natl` Acad Sci USA *99*, 12589-12593.

Bermúdez i Badia, S., Pyk, P. and Verschure, P.F.M.J. (2005). A Biologically Inspired Flight Control System for a Blimp-based UAV. Paper presented at: Proc. of the IEEE I Conf on Robotics and Automation (ICRA 2005) (Barcelona, Spain).

Bermúdez i Badia, S., Verschure, P.F.M.J. (2004). A Collision Avoidance Model Based on the Lobula Giant Movement Detector of the Locust. Paper presented at: Proc. of the I Joint Conf on Neural Networks 2004 (IJCNN'04) (Budapest, Hungary).

Bernardet, U., Blanchard, M.J. and Verschure, P.F.M.J. (2002). IQR: A distributed system for real-time real-world neuronal simulation. Neurocomputing *44-46*, 1043-1048.

Bromenshenk, J. J., Henderson C.B., Seccomb, R.A., Rice, S.D., Etter, R.T., Bender S.F.A., Rodacy, P.J., Shaw, J.A., Seldomridge, N.L., Spangler, L.H., Wilson, J.J. (2003). Can Honey Bees Assist in Area Reduction and Landmine Detection? J of Mine Action, http://maic.jmu.edu/J/7.3/focus/bromenshenk/bromenshenk.htm.

Bruschini, C., and Gros, B. (1998). A Survey of Research on Sensor Technology for Landmine Detection. J of Humanitarian Demining *2*.

Cardé, R. T., and Hagaman, T. E. (1979). Behavioral responses of the gypsy moth in a wind tunnel to air-borne enantiomers of disparlure. Environ Entomol *8*, 475-484.

Christensen, J., Pedersen, M., Aasted, B., and Alexandersen, S. (1995). Purification and characterization of the major nonstructural protein (NS-1) of Aleutian mink disease parvovirus. J Virol *69*, 1802-1809.

Christensen, T. A., and Hildebrand, J. G. (1987). Male-specific, sex pheromone-selective projection neurons in the antennal lobes of the moth Manduca sexta. J Comp Physiol [A] *160*, 553-569.

Christensen, T. A., Waldrop, B. R., Harrow, I. D., and Hildebrand, J. G. (1993). Local interneurons and information processing in the olfactory glomeruli of the moth Manduca sexta. J Comp Physiol [A] *173*, 385-399.

Eickhoff, M., Schalwig, J., Steinhoff, G., Weidemann, O., Görgens, L., Neuberger, R., Hermann, M., Baur, B., Müller, G., Ambacher, O. and Stutzmann, M. (2003). Electronics and sensors based on pyroelectric AlGaN/GaN heterostructures - Part B: Sensor applications. Physica Status Solidi *0*, 1908-1918.

Fjellanger, R., Andersen, E. and McLean, I. (2002). A training program for filter-search mine detection dogs. I J of Comparative Psychology *15*, 277-286.

Gonzalez de Santos, P., Garcia, E., Estremera, J. and Armada, M. A. (2002). SILO6: Design and configuration of a legged robot for humanitarian

demining. Paper presented at: IARP, Workshop on Robots for Humanitarian Demining (Vienna, Austria).

Gooneratne, C., Mukhopadhyay, S.C. and Sen Gupta, G. (2004). A review of Sensing Technologies for Landmine Detection: Unmanned Vehicle Based Approach. Paper presented at: The second I Conf on Autonomous Robots and Agents (Palmerston North, New Zealand).

Habib, M. K. (2002). Mine Clearance Techniques and Technologies for Effective Humanitarian Demining. J of Mine Action.

Hansson, B. S. (2002). A bug's smell--research into insect olfaction. Trends Neurosci *25*, 270-274.

Hansson, B. S., Christensen, T. A., and Hildebrand, J. G. (1991). Functionally distinct subdivisions of the macroglomerular complex in the antennal lobe of the male sphinx moth Manduca sexta. J Comp Neurol *312*, 264-278.

Kanzaki, R., Arbas, E. A., Strausfeld, N. J., and Hildebrand, J. G. (1989). Physiology and morphology of projection neurons in the antennal lobe of the male moth Manduca sexta. J Comp Physiol [A] *165*, 427-453.

Kennedy, J. S., Marsh, D. M., and Ludlow, A. R. (1978). Anemotactic zigzagging flight in male moths stimulated by pheromone. Physiological Entomology *3*, 221-240.

Lei, H., and Hansson, B. S. (1999). Central processing of pulsed pheromone signals by antennal lobe neurons in the male moth Agrotis segetum. J Neurophysiol *81*, 1113-1122.

Lilienthal, A., and Duckett, T. (2003). Experimental Analysis of Smelling Braitenberg Vehicles. Paper presented at: Proceedings of the IEEE I Conf on Advanced Robotics (ICAR 2003) (Coimbra, Portugal).

Lilienthal, A. J., and Duckett, T. (2004). Experimental Analysis of Gas-Sensitive Braitenberg Vehicles. Advanced Robotics *18*, 817-834.

Marques, L., Rachkov, M., de Almeida, A.T. (2002). Mobile pneumatic robot for demining. Paper presented at: I Conf on Robotics and Automation.

Milne-Thomson, L. M. (1973). Theoretical Aerodynamics (New York, Dover Publications).

Mishima, T., and Kanzak, R. (1998). Coordination of flipflopping neural signals and head turning during pheromone-mediated walking in a male silkworm moth Bombyx mori. J Comp Physiol A *183*, 273-282.

Murlis, J., and Jones, C. (1981). Fine scale structure of odor plumes in relation to insect orientation to distant pheromone and other attractant sources. Physiol Ent *6*, 71-86.

Murlis, J., Elkinton, J. S., and Carde, R. T. (1992). Odor plumes and how insects use them. Annu Rev Ent *37*, 505-532.

Nanto, H., and Stetter, J. R. (2003). Introduction to Chemosensors. In Handbook of Machine Olfaction, T. C. Pearce, S. S. Schiffman, H. T. Nagle, and J. W. Garnder, eds. (Weinheim, Wiley-VCH), pp. 79-103.

Nelson, R. (1989). Flight stability and automatic control (New York, McGraw-Hill).

Neubecker, A., Pompl, T., Doll, T., Hansch, W. and Eisele, I.s (1997). Ozone-enhanced molecular beam deposition of nickel oxide (NiO) for sensor applications. Thin Solid Films *310*, 19-23.

Nicoud, J. D., and Habib, M.K. (1995). The Pemex-B autonomous demining robot: perception and navigationstrategies. Paper presented at: I Conf on Intelligent Robots and Systems (Pittsburgh, PA, USA).

O'Dwyer, A. (2003). Handbook of PI and Pid Controller Tuning Rules (London, Imperial College Press).

O'Malley, T. J. (1993). Seek and Destroy - Clearing Mined Land. Armada I *1*, 6-15.

Olberg, R. M. (1993). Pheromone-triggered flip-flopping interneurons in the ventral nerve cord of the silkworm moth, Bombyx mori. J Comp Phys [A], 297-307.

Pearce, T. C., Chonga, K.Y., Verschure, P.F.M.J., Bermúdez i Badia, S., Carlsson, M.A., Chanie, E., Hansson, B.S. (2004). Chemotactic search in complex environments: From insects to real-world applications. In Electronic Noses & Sensors For The Detection Of Explosives, J. W. Gardner, and J. Yinon, eds. (Dordrecht/Boston/London, Kluwer Academic Pub), pp. 181-207.

Pyk, P., Bermúdez i Badia, S., Bernardet, U., Knuesel, P., Carlsson, M.A., Gu, J., Chanie, E. , Hansson, B.S., Pearce, T.C., Verschure, P.F.M.J. (2006). An artificial moth: Chemical source localization using a robot based neuronal model of moth optomotor anemotactic search. Autonomous Robots *20*, 197-213.

Rose, A., Zhu, Z., Madigan, C. F., Swager, T. M., and Bulovic, V. (2005). Sensitivity gains in chemosensing by lasing action in organic polymers. Nature *434*, 876-879.

Santana, P., and Barata, J. (2005). Unmanned Helicopters Applied to Humanitarian Demining. Paper presented at: Emerging Technologies and Factory Automation.

Verhagen, R., Weetjens, F., Cox, C., Weetjens, B. and Billet, M. (2006). Rats to the Rescue: Results of the First Tests on a Real Minefield. J of Mine Action *9.2*, http://www.maic.jmu.edu/J/9.2/RD/verhagen/verhagen.htm.

Vickers, N. J., and Baker, T. C. (1994). Reiterative responses to single strands of odor promote sustained upwind flight and odor source location by moths. Proc Natl Acad Sci USA *91*, 5756-5760.

Wada, S., and Kanzaki, R. (2005). Neural control mechanisms of the pheromone-triggered programmed behavior in male silkmoths revealed by double-labeling of descending interneurons and a motor neuron. J Comp Neurol *484*, 168-182.

Zufferey, J. C., Guanella, A., Beyeler, A. and Floreano, D. (2006). Flying over the reality gap: From simulated to real indoor airships. Autonomous Robots *21*, 243-254.